Design and Performance of a 600−720-GHz Sideband-Separating Receiver using AlO_x and AlN SIS Junctions.

F. P. Mena, J. W. Kooi, A. M. Baryshev, C. F. J. Lodewijk, T. Zijlstra, R. Hesper, G. Gerlofsma, T. M. Klapwijk, and W. Wild

***Abstract*—We present the design, modeling, construction, and characterization of a sideband separating heterodyne receiver that covers the frequency range from 600 to 720 GHz. The receiver has been constructed using waveguide technology in the split-block technique. The core of the mixer consists of a quadrature hybrid, two directional couplers to inject the local oscillator signal, two superconductor-insulator-superconductor (SIS) junctions, three signal-termination loads, and two planar intermediate-frequency/bandpass-filter/dc-bias circuits. The instrument that we have constructed presents excellent performance as demonstrated by two important figures of merit; receiver noise temperature and sideband ratio. Across the entire band, the uncorrected single-sideband noise temperature is below 500 K and reaches 190 K at the best operating point. The sideband ratio is greater than 10 dB over most of the frequency operating range. Superconducting junctions containing AlO_x- and AlN-tunnel barriers were tested.**

I. Introduction

The Atacama Large Millimeter Array (ALMA) is the largest radio astronomical enterprise ever proposed. Currently, ALMA is under construction and is expected to be fully operational by 2012 [1]. When completed, each of its more than 60 constituent radio-telescopes will include 10 heterodyne receivers covering the spectral windows allowed by the atmospheric transmission at ALMA's construction site, the altiplanos of the northern Chilean Andes. In contrast to the sideband-separating receivers being developed at low frequencies [1], [2], [3], [4], double-sideband (DSB) receivers are being developed for the highest two spectral windows (bands 9 [5] and 10 [6]).

In the DSB detection mode, the signal to be detected (RF) is mixed, in a non-linear device, with a well-determined reference signal called local oscillator (LO). As a result, the RF signal is down converted to an intermediate frequency (IF), $\omega_{IF} = |\omega_{RF} - \omega_{LO}|$. This down conversion process allows further study of the signal in a more manageable frequency range (usually a few GHz). It is evident that DSB mixers cannot distinguish between signals at frequencies above or below the LO frequency signal, known as upper (USB) and lower (LSB) sidebands, respectively. To circumvent this problem it is possible to suppress one of the sidebands before it is fed into the mixer. This, however, requires extra instrumentation, such as a bandpass filter, in front of the mixer. A more frequency agile solution is a sideband-separating mixer, which produces two IF outputs corresponding to the two sidebands. As a trade off, this solution does require extra RF components *inside* the mixer, the design of which are outlined in this paper.

The characteristic that sideband-separating mixers distinguish between the image and signal sidebands can be exploited in astronomy by providing enhanced atmospheric noise reduction when compared with DSB receiving techniques. When the astronomical spectral line of interest is located in one of the sidebands, atmospheric noise present in the image sideband is not folded with the signal sideband as would be the case with a DSB mixer, thus allowing for a lower system noise temperature. Despite this advantage, sideband-separating mixers have not been implemented in the highest-frequency bands of ALMA because of the small (waveguide) dimensions required for the RF components inside the mixer. However, advances in state-of-the-art micromachining technology now achieve the accuracies necessary to realize this development [7]. In this paper we report the design, modeling, construction, and characterization of a sideband-separating mixer that covers the frequency range from 600 to 720 GHz corresponding to band 9 of ALMA. The receiver we have constructed has excellent performance, both in sensitivity and sideband rejection. Across the entire band the uncorrected single-sideband noise temperature is less than 500 K and reaches 190 K at the best operating point. In addition, the sideband ratio is greater than 10 dB over 95% of the frequency range. With those values, the mixer accommodates ALMA specifications [8] at most operating frequencies. Incremental progress reports of this work have been presented in several conference proceedings [9], [10], [11], [12]. Here, we present a comprehensive summary and extend it in two ways: First, we have completed our simulations to understand the operation of the receiver and, secondly, we have tested the performance with a pair of AlN-barrier SIS junctions. Both can orient future work on improving the performance of this and similar

F. P. Mena, A. M. Baryshev, R. Hesper, G. Gerlofsma, and W. Wild are with the Netherlands Institute for Space Research (SRON) and the Kapteyn Institute, University of Groningen, Landleven 12, 9747 AD Groningen, The Netherlands. F. P. Mena is now with the Department of Electrical Engineering, Universidad de Chile, Av. Tupper 2007, Santiago, Chile.

J. W. Kooi is with the California Institute of Technology, MS 320-47 Pasadena, California 91125, USA

C. F. J. Lodewijk, T. Zijlstra, and T. M. Klapwijk are with the Kavli Institute of Nanoscience, Delft University of Technology, Lorentzweg 1, 2628 CJ Delft, The Netherlands

We gratefully acknowledge funding from NOVA, the Netherlands Research School for Astronomy, and the the European Community's sixth Framework Programme under RadioNet R113CT 2003 5058187. A. Baryshev also acknowledges support by a grant from the STW/NWO (VENI 08119).

[1][Online]. Available: http://www.alma.nrao.edu.

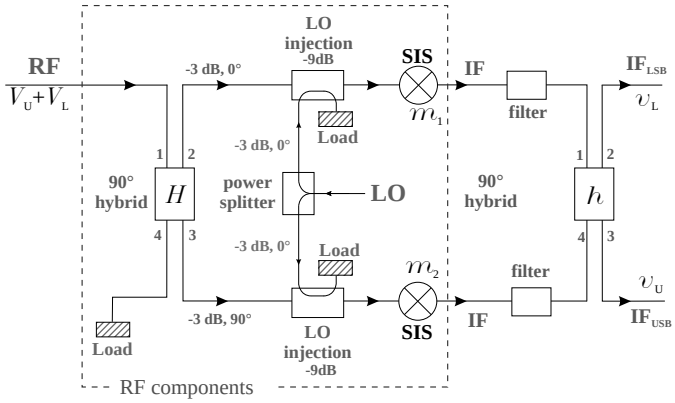

Fig. 1. Schematic of the selected sideband-separating configuration. The incoming RF signal ($V_U + V_L$) is divided in a 90° hybrid resulting in two branches having the same amplitude but differing 90° in phase. The branches are then combined with a LO signal and mixed into two non-linear-response devices (SIS junctions in our case). The resulting down converted signals are fed into a second quadrature hybrid, after which the IF signals corresponding to the upper and lower sideband (v_U and v_L) are obtained in the two separate IF output channels.

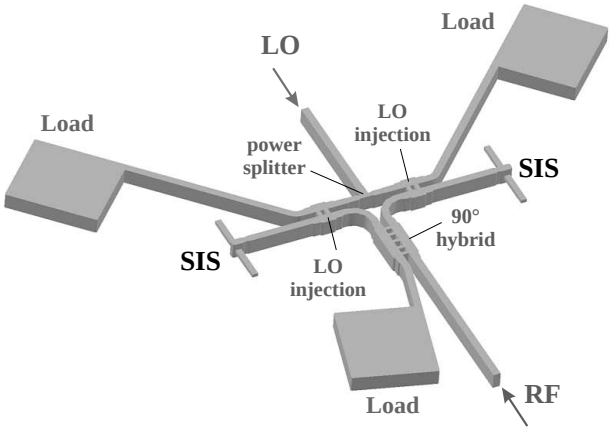

Fig. 2. Proposed realization of the RF components schematically indicated in Fig. 1. These components are designed in full-height waveguide. In the design 12 % of the RF signal and 88 % of the injected LO are routed to the terminating loads. The transverse waveguide dimensions are; $a = 310$ μm and $b = 145$ μm.

TABLE I
WAVEGUIDE DIMENSIONS OF FIG. 3

Element	a_1	a_2	a_3	a_4	a_5	a_6	a_7
Dimension (μm)	168	198	120	130	90	160	270

Element	c_1	c_2	c_3	s_1	s_2
Dimension (μm)	102	120	76	71	82

receivers.

II. Design and Modeling

A. General Concept and Model

From a variety of possible sideband-separating schemes, we have selected the configuration shown in Fig. 1. The RF signal to be detected can be represented as a superposition of signals above, V_U, and below, V_L, the LO frequency. This signal is coupled to a quadrature hybrid which splits the signal into two branches of (approximately) equal amplitude and 90° phase separation. Each branch is then coupled with the LO signal and mixed (multiplied) into a non-linear device. The two resulting IF signals are coupled to a second 90° hybrid whose outputs are v_U and v_L. In a perfect scenario these outputs contain the desired upper and lower sidebands. If perfect terminating loads are assumed, this process can be described as

$$\begin{aligned} v_U &= g_{1U}V_U + g_{1L}V_L^* \\ v_L &= g_{2U}V_U + g_{2L}V_L^* \end{aligned} \quad (1)$$

where

$$\begin{aligned} g_{1U} &= h_{31}m_1H_{21} + h_{34}m_2H_{31} \\ g_{2U} &= h_{21}m_1H_{21} + h_{24}m_2H_{31} \\ g_{1L} &= h_{31}m_1H_{21}^* + h_{34}m_2H_{31}^* \\ g_{2L} &= h_{21}m_1H_{21}^* + h_{24}m_2H_{31}^* \end{aligned}$$

In these equations, m_i, H, and h represent the transmission coefficient of non-linear device i after LO injection, and the transmission matrices of the RF and IF hybrids, respectively. This model will be used in Section II-D.

Superconductor-insulator-superconductor (SIS) junctions, as detailed in Section II-C, are used as non-linear mixing elements. Because of the intrinsic parasitic capacitance of SIS junctions, intermodulation products and higher harmonics are naturally suppressed. Therefore, a 90° RF hybrid can be used instead of a 180° hybrid, despite the latter having superior fundamental and intermodulation product suppression capabilities. Moreover, a 90° hybrid is simpler to construct and thus easier to implement at these high frequencies [13].

In the implementation of the mixer we have opted for waveguide technology in the construction of the RF components (Section II-B), and planar stripline for the IF filtering and matching parts (Section II-E). The entire design is based on an analytical model [14], and verified by HFSS [15] and Microwave Studio [16]. The dimensions of each RF component were adjusted for optimal performance in the $600 - 720$ GHz range, while the IF components are optimized for $4 - 8$ GHz.

B. RF Components

For implementation of the RF circuitry we have selected the design presented in Fig. 2. Note that this figure represents the channels to be machined into the split mixer blocks. The coupling sections, shown in detail in Fig. 3*a*, are based on a narrow bandwidth split block version developed for the ALMA project at lower frequencies [17]. Here, however, the waveguide widths in the hybrid and the LO couplers have been increased by 36.5 % to maximize the thickness of the branch lines[13], thereby easing machining constraints. This width increase is the maximum limit before the TE_{01} mode gets excited at the high end of the frequency band. Each of these components was simulated and optimized using commercial software [15], [16]. The geometric parameters are summarized in Table I. Some selected S-parameters obtained from the design process are depicted as solid lines in Fig. 3*b*. These

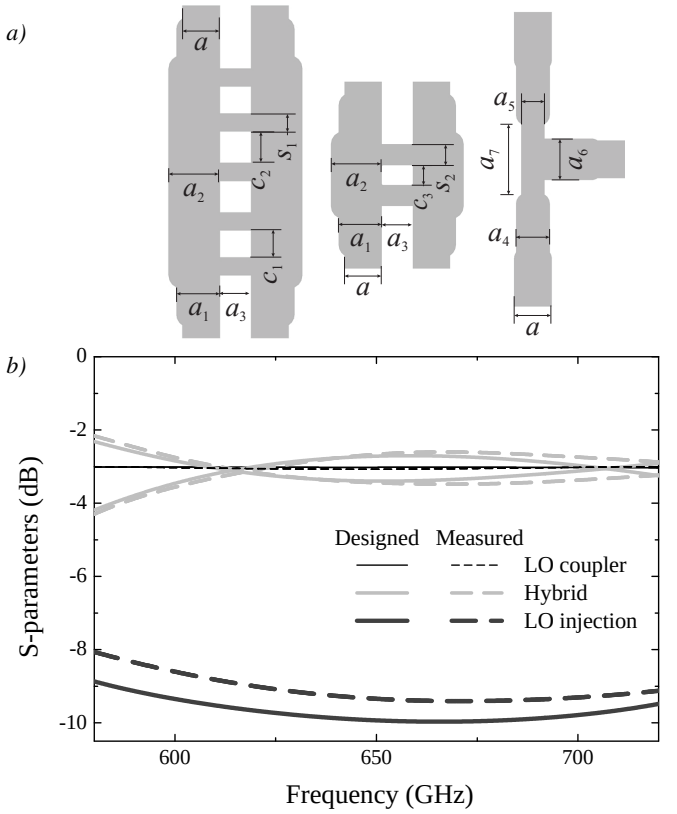

Fig. 3. *a)* Detailed top views of the 90° RF hybrid (left), LO coupler (center), and LO power splitter (right). Note that in the hybrid and LO coupler, the width (a_2) of the waveguide is increased in the proximity of the branch lines to maximize the spacing s_1 and s_2. All components are drawn to scale. For dimensions see Table I. *b)* Calculated S-parameters between the input and output as designed (solid lines) and as measured (dashed lines) [7].

TABLE II
GEOMETRIC PARAMETERS OF THE TERMINATION LOAD SHOWN IN FIG. 4

Element	a_1	c_1	c_2
Dimension (μm)	1650	1800	300

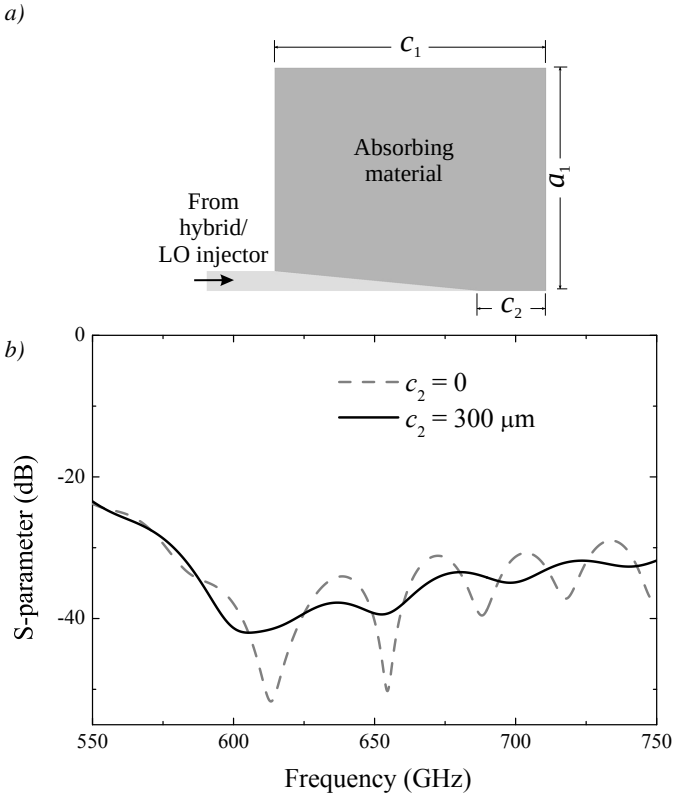

Fig. 4. *a)* Detailed view of the terminating load. A rectangular cavity ($a_1 \times c_1$) with the same depth of the waveguide is machined at the end of the waveguide and partially filled with a wedged piece of absorbing material. For dimensions see Table II. *b)* Simulated reflection coefficient of the load in two different cases, $c_2 = 0$ μm (dashed line) and $c_2 = 300$ μm (solid line).

TABLE III
GEOMETRIC PARAMETERS OF THE WAVEGUIDE-TO-SIS TRANSITION SHOWN IN FIG. 5

Element	Dimension (μm)
Quartz substrate	$50 \times 100 \times 1585$
Air height below substrate	50
Air height above substrate	25
Capacitive step width	118
Capacitive step length	70
Backshort radius	35
Distance backshort-substrate	59
Radius radial probe	84
RF choke (high impedance)	65×65
RF choke (low impedance)	5×72

show a rather flat response in our frequency window (600 - 720 GHz).

Although several configurations have been proposed for the signal termination loads [17], [18], we have selected a rather novel and simple configuration which is appropriate for the small dimensions involved in the present work. The design, presented in Fig. 4*a*, consists of a cavity at the end of the waveguide partially filled with an absorbing material. Since the longest dimensions of this geometry are parallel to the splitting plane of the block, this cavity and the filling material are relatively easy to machine compared to other geometries. Extensive simulations of this configuration have been presented elsewhere [9]. If Eccosorb MF112 [19] is used as absorbing material, the load shows excellent performance, as demonstrated by the reflection coefficient (Fig. 4*b*). When the cavity is terminated at the point where the wedged part ends ($c_2 = 0$), large resonances appear. They can be easily damped by adding extra absorbing material. We have constructed the termination loads with $c_2 = 300$ μm as they provide the maximum damping [9]. Moreover, it has also been shown that this configuration is reasonably robust as various mounting errors have little influence in the overall performance.

The combined RF-LO signal is coupled to the thin-film tuning structure of the SIS junction via a radial-probe based full-height waveguide-to-microstrip transition, as shown in detail in Fig. 5*a*. In this transition, the waveguide backshort has a radius of 35 μm and is spatially located 59 μm from the edge of the quartz substrate. The overall performance of the coupling is improved by adding a capacitive step in front of the substrate [20]. The use of an "across-the-waveguide" probe configuration facilitates biasing the junction and extraction of the IF signal. Care must be taken however in the way the opposite sides of the waveguide are connected as the meandering transmission line is prone to excite resonances

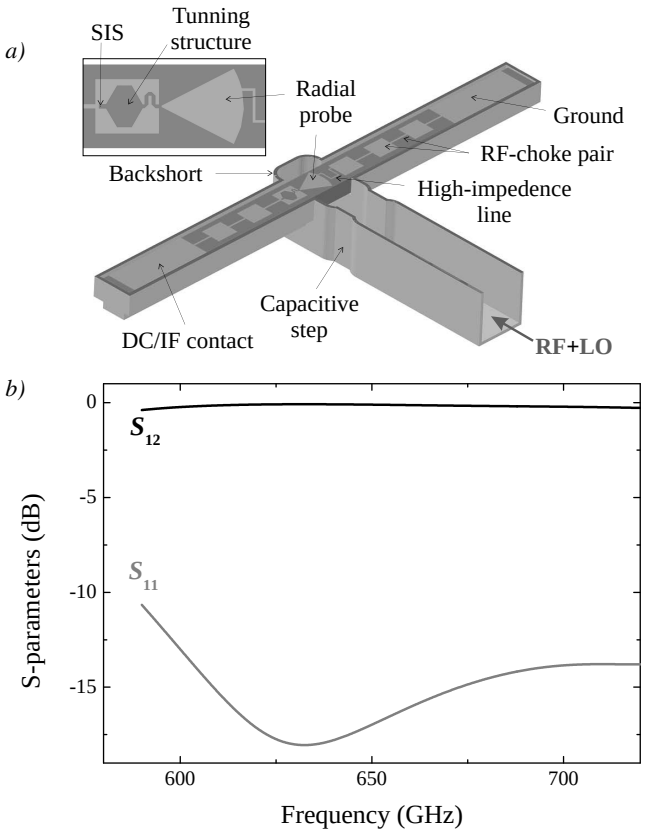

Fig. 5. *a)* Detailed views of the waveguide-to-microstrip transition and of the RF tuning structure. The combined RF-and-LO signal is brought into the SIS junction via a radial probe and RF matching network. The superconducting RF choke is used to bring out the IF signal from the SIS junction and to provide bias. The most important dimensions are given in Table III and the material properties in Table VI. *b)* Coupling efficiency (S_{12}) and return loss (S_{11}) between the waveguide input and the tip of the radial probe (tuning structure and SIS junction not included in this simulation).

TABLE IV
DIMENSIONS (IN μM) OF THE RF TUNING STRUCTURE BASED ON A 40 Ω WAVEGUIDE TRANSITION IMPEDANCE. THE LAYOUT IS SHOWN IN THE INSET OF FIG. 6

Junction	L_1	L_2	L_3	L_{tap}	W_1	W_2	W_3
AlO_x	5.0	41.5	44.0	12.45	5.5	50.0	4.5
AlN	14.2	22.4	50.9	2.23	3.2	18.0	3.0

[21]. The whole structure was simulated and optimized with commercial software [16]. Table III summarizes the obtained dimensions. In Fig. 5*b* we present the calculated coupling efficiency, and input return loss, between the waveguide and the throat of the radial probe.

C. SIS Junction and RF Tuning Structure

At the beginning of this project, we were faced with the option of selecting Nb/AlO_x/Nb or Nb/AlN/Nb junctions for our design. On one hand, SIS junctions with AlN tunnel barriers and high current density (J_c) have intrinsically better properties [22] but the process of fabrication was still under development at Delft University of Technology although with excellent perspectives [23]. On the other hand, the fabrication process of Nb/AlO_x/Nb junctions was more mature as evidenced by our

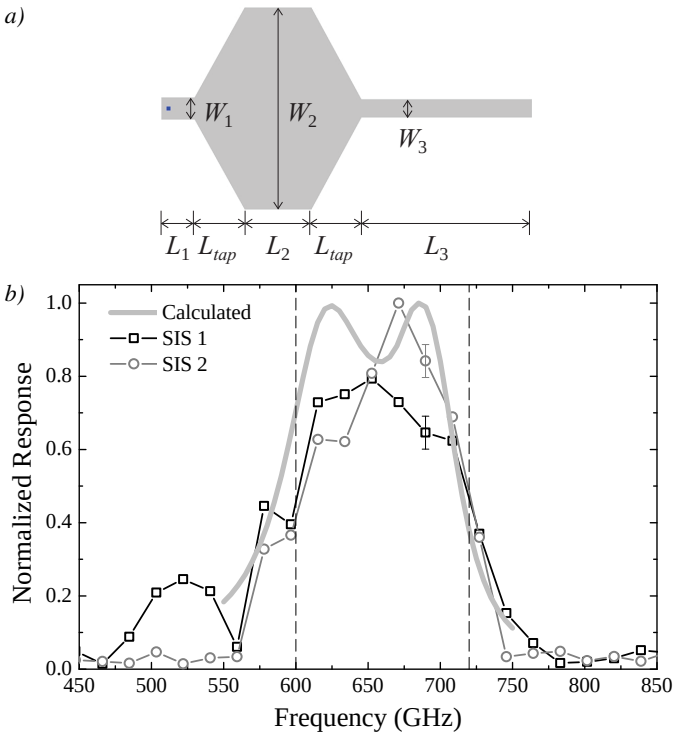

Fig. 6. *a)* Thin-film tuning structure between the SIS junction and the tip of the radial probe. Dimensions are given in Table IV. The same kind of structure was used with the AlN junctions. Note that, when necessary, L_3 has been meandered to fit in the actual fabricated device. *b)* Calculated (includes the waveguide transition) and measured direct detection response of the fabricated AlO_x SIS junctions. Typical error bars of the experiment are also shown. Vertical dashed lines show the band 9 range.

successful experience with the development of DSB receivers for band 9 of ALMA [5]. As a compromise, we baselined AlN junctions for our design with the hope that AlO_x junctions could also be tested inside of the same structure, albeit with non-optimized parameters. This is an important detail in our discussion of the experimental results as this specificity is reflected in the design of the planar IF filter of Sec. II-E.

The other important design selection we made is the choice of a single junction approach. The reasons for this choice are two-fold. It facilitates higher uniformity, important to the balance in the sideband separation mixer, and secondly, it allows to suppress more easily the Josephson currents through the tunnel barrier.

Following [24] and [25], it was decided to terminate the SIS junction into a load of $\sim 2R_n$ to achieve the required 8-GHz IF bandwidth [8]. Expecting 10 Ω normal state resistance AlN-barrier tunnel junctions ($J_c \sim 25$ kA/cm^2) the IF termination impedance at the junction was designed to be 20 Ω (Sec. II-E). However due to initial fabrication difficulties lower current density AlO_xbarrier tunnel junctions (J_c = 9 kA/cm^2) were used instead for much of the measurement campaign. These mixing devices are similar to the ALMA band 9 SIS junctions, which are designed to directly contact a 50 Ω SMA IF output connector ($R_n \sim 20$ Ω), thereby providing a non-optimal IF termination.

The geometric capacitance of SIS junctions is another matter, the reactance being significant at the RF frequencies

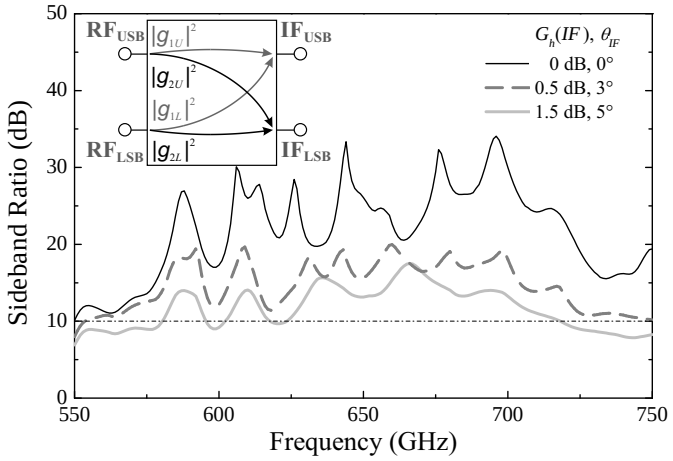

Fig. 7. Calculated sideband ratio assuming different amplitude and phase imbalances of the IF hybrid. The horizontal dotted line represents the ALMA specifications as described in the text. For the calculations we have assumed a mixer imbalance (G_m) of 0.25 dB and the chip misalignment phase error (φ) of 5°. *Inset:* Definition of gains between the different ports necessary to define the sideband ratios. In our model, both sideband ratios are equal.

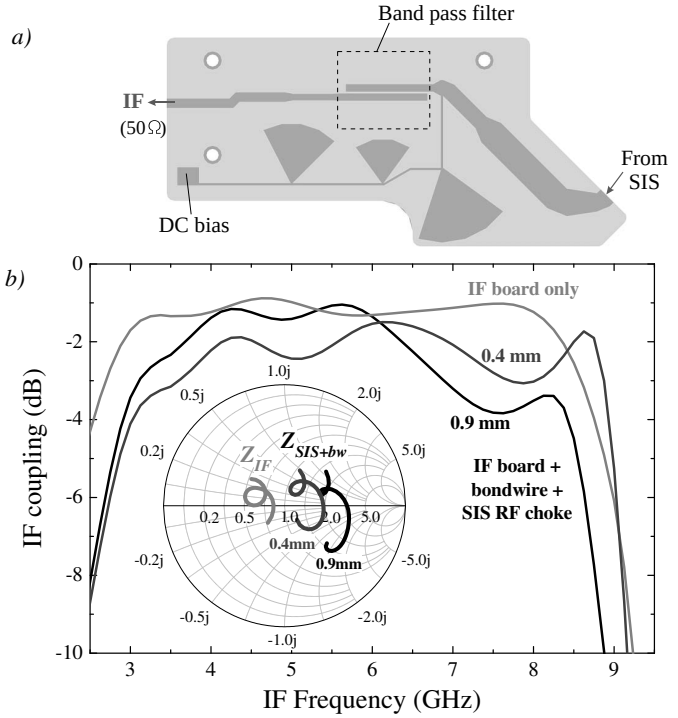

Fig. 8. *a)* Realization of the planar-stripline IF system. The connection to the SIS junction is accomplished via a (inductive) bond-wire. The dashed line shows the positioning of a cutout bellow the substrate needed for the $3-9$ GHz band pass filter. *b)* Calculated transmission between the input and output ports of the IF structure. *Inset:* Complex impedances, from 4 to 8 GHz, at the input of the IF board (Z_{IF}) and at the SIS tunnel junction (Z_{SIS+bw}). The Smith chart is normalized to 50 Ω. See text for details.

we concern ourselves with. Combined with the LO-pumped quantum susceptance [26] it shunts the relatively constant impedance of the radial probe waveguide-to-microstrip transition of Fig. 5. To optimize coupling efficiency to the waveguide over an as large as possible RF bandwidth we have employed, for both the AlO_x and AlN SIS junction designs, an 'end-loaded' stub [27] radial probe matching network. The geometric parameters (inset Fig. 6) were tuned to get good coverage from 600-720 GHz [27]. For the AlO_x and AlN junction designs the dimensions of the RF matching network are provided in Table IV. The calculated transmission (thick solid line) overlaid on the measured direct detection response is shown in Fig. 6.

D. Sideband Ratio

An important parameter characterizing a sideband-separating mixer is the so-called sideband ratio. Following (1) and the inset of Fig. 7, the sideband ratio for a given channel is defined as the ratio between the gains coming from the two input ports, *i.e.*

$$R_{USB} = \frac{|g_{1U}|^2}{|g_{1L}|^2}\ , \quad R_{LSB} = \frac{|g_{2L}|^2}{|g_{2U}|^2} \tag{2}$$

In a perfect sideband separating mixer, these ratios are infinity. However, imperfection of the different components reduce this value. This quantity can be modeled by considering the different transmission coefficients of RF and IF hybrids and SIS junctions given in (1). These coefficients can be written as

$$\begin{aligned} H_{21} = \tau_{RF} e^{-i\theta_{RF}} \quad &, \quad H_{31} = \rho_{RF} e^{-i\pi/2} \\ h_{21} = h_{34}^* = \tau_{IF} e^{-i\theta_{IF}} \quad &, \quad h_{31} = h_{24}^* = \rho_{IF} e^{-i\pi/2} \\ m_1 = a e^{-i\varphi} \quad &, \quad m_2 = b \end{aligned}$$

where τ and ρ represent the amplitude imbalance of the hybrids, θ their phase imbalances, a and b the conversion gain of the junction(s), and φ the phase error introduced by chip misalignment in the waveguide. Given these coefficients, the sideband ratios can be rewritten as

$$R_{USB} = R_{LSB} = -10\log\left(\frac{1-2\sqrt{G}\cos\phi+G}{1+2\sqrt{G}\cos\phi+G}\right) \tag{3}$$

Here, G is the product of the mixer gain imbalance, $G_m = |a/b|^2$, and the imbalance of the two hybrids, $G_h = |\rho/\tau|^2$. The total phase error is accounted for by $\phi = \theta_{RF}+\theta_{IF}+\varphi$. In Fig. 7 we show the sideband ratio calculated according to (3) for different values of $G_h(IF)$ and θ_{IF}. For these calculations we have set $G_m = 0.25$ dB, the mixer phase error (due to mounting of the individual SIS junctions) $\varphi = 5°$, with $G_h(RF)$ and θ_{RF} derived from the calculated transmission coefficients of the RF hybrid and the coupling between the radial probe and the SIS junction. If a perfect IF hybrid is assumed, a sideband ratio larger than 20 dB is expected across the entire band. This sets the upper limit for the performance of the present mixer. A more realistic situation is obtained if some imbalance is added. This results in a degraded sideband ratio as shown in Fig. 7.

TABLE V
PARAMETERS OF THE IF-DC BLOCK/BANDPASS FILTER SHOWN IN FIG. 8

Substrate material	Alumina
Dielectric constant	9.8
Substrate heigth (μm)	635
Coupled lines width (μm)	480
Coupled lines length (mm)	5.72
Spacing between coupled lines (μm)	120
Cavity (mm)	$0.585 \times 5.08 \times 6.1$
Air height above substrate (mm)	2.5

E. Planar IF filter

To facilitate reliability, modeling, and repeatability, we have opted for a planar IF design (Fig. 8*a*). This is a compact unit containing the IF match, dc-break, bias tee, and EMI filter. At the heart of the structure there is a pair of parallel coupled suspended transmission lines [28]. By removing part of the ground underneath the transmission lines, as indicated in Fig. 8*a*, a $3-9$ GHz band pass filter is formed. The advantage of such planar structure has been demonstrated and used in various astronomical instruments [13], [29]. An added advantage of the planar approach is homogeneity as this helps minimize the differential phase error at the mixer IF output. The IF circuit, one per SIS mixer, is mounted in cavities milled out in the split block (see Fig. 9*b*) and connected to the junction via bond wires.

The entire IF structure has been designed in Microwave Office [14] and HFSS [15] and employs as substrate material alumina (ϵ_r=9.8) with a height of 635 μm. The dimensions of the coupled lines (Table V) were optimized to cover the 4 to 8 GHz frequency range. In the design of the IF matching network we have taken into account the combined geometric and thin-film microstrip capacitance of the junction, the RF choke, the wire bond inductance that connects the SIS chip to the IF board, and the SIS normal resistance, R_n. The calculated total parasitic capacitance is 307 fF, with the inductance of the bond wire determined by its length. In the modeling we have assumed a bond wire length of 0.3-0.4 mm. Following the discussion in Sec. II-C, R_n was taken to be 10 Ω, considering availability of AlN junctions [23]. The results of the simulations are summarized in Fig. 8*b*. For comparison, we present also the transmission of only the IF planar circuit and of the complete system with two different lengths of bond wires. The wirebond inductance (L) and combined parasitic junction capacitance (C) act to transform the IF impedance (Z_{SIS+bw} in Fig. 8), thereby reducing the available IF bandwidth. For a 0.9 mm wirebond length the highest IF frequency is approximately 7 GHz, whereas for a 0.4 mm wirebond length this limit is pushed to about 8.75 GHz. Note also that the apparent 1 dB loss in coupling efficiency is the result of absorption loss in the alumina substrate (loss tangent = 0.002). At cryogenic temperatures the substrate loss is expected to reduce to about 0.3 dB.

III. CONSTRUCTION

A. Waveguide Block

We have constructed the mixer in a split-block configuration as demonstrated in Fig. 9. Conventional machining was used

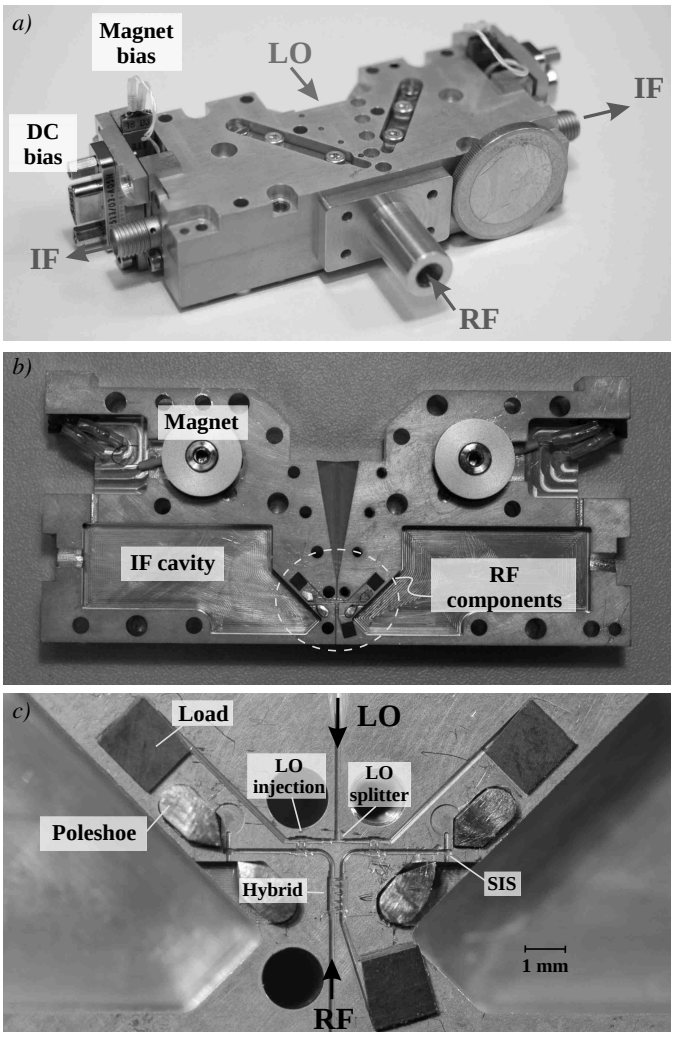

Fig. 9. Constructed sideband-separating block and its different components. *a)* Final assembly of the block. *b)* Upper half-block showing the defluxing magnets, cavities for the IF board, and the RF components. *c)* Close up of the different RF components mounted in the upper block. Note that the SIS junctions and the IF board are mounted in the bottom block which is not shown here.

for the large structures and computer numerically controlled (CNC) micro-machining for the small RF features [7]. Both parts of the block were made of copper which were gold plated afterwards to a thickness of approximately 2 μm. The fabricated unit is rather compact ($8\times2\times3$ cm^3), it contains all the RF components, the IF filtering board, the dc bias circuit, and the magnetic probes needed to suppress the Josephson currents in the SIS junctions. A closer inspection of the fabricated block shows that all the waveguides and cavities are approximately 5 μm wider than designed. The reason appears to be etching of the copper block during the gold plating process. However, the erosion is rather uniform through the entire block. To determine the influence of wider waveguide dimensions, we have repeated the simulation process with the measured dimensions (dashed lines in Fig. 3). It is clear that our design is reasonably robust as long as the symmetry of the RF components is maintained. We also like to point out that a rather recent fabrication process based on photolithography

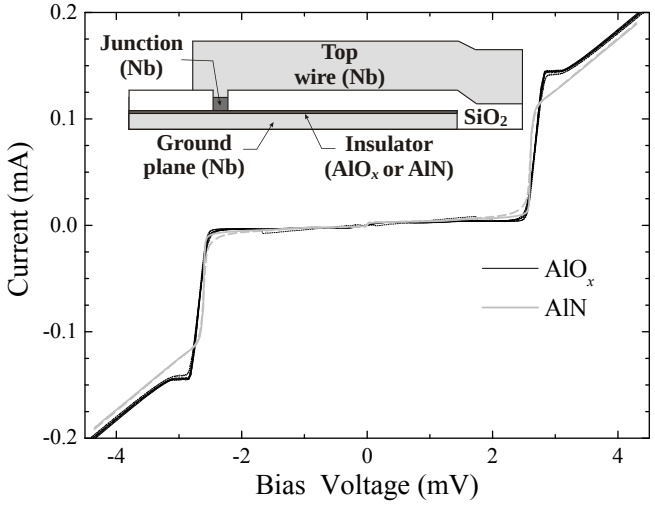

Fig. 10. I-V curves of eight different AlO_x (black thin lines) and two AlN (thick gray lines) before mounting them on the split block. *Inset:* Cross section of the SIS junction and tuning structure (not drawn to scale).

TABLE VI
SIS PARAMETERS

Parameter	Design		Experimental	
	AlO_x	AlN	AlO_x	AlN
V_g (mV)	2.7	2.7	2.7	2.6
R_n (Ω)	20	20	21	20
Area (μm^2)	1.0	0.36	0.95	0.4
$R_nA(\Omega\mu m^2)$	20.0	7.2	20	8
J_c(kA/cm^2)	9.5	26	9.5	23.8
C_s(fF/μm^2)	80	90	–	–
σ_{Nb} (S/m)	10^7	10^7	–	–
Nb Top (nm)	500	500	–	–
Nb Bottom (nm)	200	200	–	–
SiO_2 (nm)	250	250	–	–

can achieve the small details presented here with an accuracy of less than 1 μm [30]. If this method is combined with conventional CNC machining to implement the larger details of the block, it would permit in the future a more reliable fabrication process and its application towards even higher frequencies and/or array receivers [12].

B. SIS Junctions

The SIS devices are fabricated on a 200 μm thick quartz substrate. First, a sacrificial Nb monitor layer is deposited, followed by an optically defined trilayer of Nb/Al/AlO_x/Nb. The thickness of the Al layer is 5-7 nm, the top and bottom niobium layers are 100 nm thick. Junctions are defined by e-beam lithography using negative SAL601 resist and etched in a SF_6/O_2 reactive ion etch (RIE) plasma. The AlO_x layer acts as an etch stop for the groundplane. The junction resist pattern is subsequently used as a lift-off mask for a dielectric layer of SiO_2. A Nb/Au top layer is deposited to define the top wire and contact pads. The Au is wet-etched in a KI/I2 solution using an optically defined window. Finally, using an e-beam defined top wire mask pattern, the top-layer of Nb is etched in a SF_6/O2 RIE plasma, which finishes the fabrication process. The inset of Fig. 10 shows a schematic cross section of the fabricated device. In Table VI the parameters of the SIS junctions and RF matching network are given.

An identical process is used for junctions with AlN tunnel barriers, except for the barrier growth itself. The AlN layer is grown using a plasma source with a remote inductively coupled N_2 plasma at 4×10^{-2} mbar. The plasma source is at a distance of 10 cm. The ICP power set point is 550 W. A nitridation time of 17 min resulted in 23.8 kA/cm^2 junctions.

IV. Experiment, Results and Discussion

A. I-V Curves

The AlO_x SIS fabrication process provides high yield and good reproducibility as demonstrated by the eight I-V curves (out of a sector containing 20 identical junctions) in Fig. 10. The relevant SIS parameters are provided in Table VI. For the depicted AlO_x-barrier SIS junctions the subgap-to-normal state resistance ratio is ~ 20, and the gap smear ~ 40 μV. Two of the junctions were selected and inserted in the described sideband-separating block. After mounting, one of the devices showed an increased normal state resistance of ~ 1 Ω. This can be attributed to the silver epoxy used to make the ground contact.

The fabrication process of AlN junctions provided lower yield but did otherwise also produce junctions with excellent properties (Table VI). I-V plots of the two selected junctions, before mounting, are also shown in Fig. 10 for comparison. An important difference is the absence of the above-the-gap proximity *"knee"*, characteristic of AlO_x junctions.

B. Band Coverage

The direct response, as function of frequency, of both SIS junctions contained in our receiver has been measured using a home-made Fourier-transform spectrometer. The measurements were performed with the junctions mounted inside the mixer block and with the test signal fed through the RF port. The results for AlO_x junctions are presented in Fig. 6. Both junctions present good band coverage and are in good agreement with the predicted response. The agreement is obtained despite the fabrication issues discussed in Section III-A, as those errors do not significantly effect the impedances at the probe tip.

C. Sideband Ratio

The sideband ratios of the two IF outputs, when AlO_x junctions were inserted, were measured using the experimental set up shown schematically in Fig. 11. This configuration allows the measurement of the rejection ratios without knowledge of the RF signal levels. The IF response to broadband RF noise sources at two temperatures has to be measured however [31]. We have used a commercial microwave absorber [32] to insert the noise sources at ambient and liquid-nitrogen temperatures.

Fig. 12 shows the measured sideband ratio of every channel as function of RF and IF frequency. ALMA science specifications determine that sideband-separating channels shall provide at least 10 dB image sideband suppression [8]. In our case, it is found that 95 % of the operational bandwidth

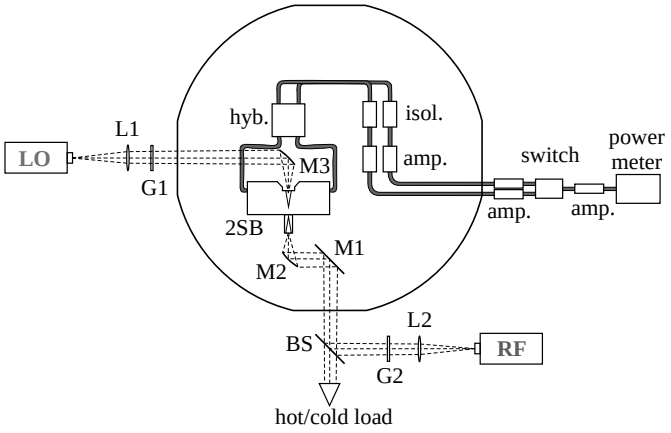

Fig. 11. Schematic of the experimental setup used to determine sideband ratios. The signals from two different sources are brought into the sideband separating mixer (2SB) by means of a combination of lenses and mirrors (L1, L2, M1, M2, and M3). The intensities of the sources can be regulated with the metal grids G1 and G2, respectively. A hot/cold load is also fed into the mixer using a chopper which selects between them. If the beam splitter (BS) is removed, the same configuration can be used to determine noise temperatures. The figure also shows how the IF chain (hybrid, isolators, amplifiers, and switch) were connected during the experiments.

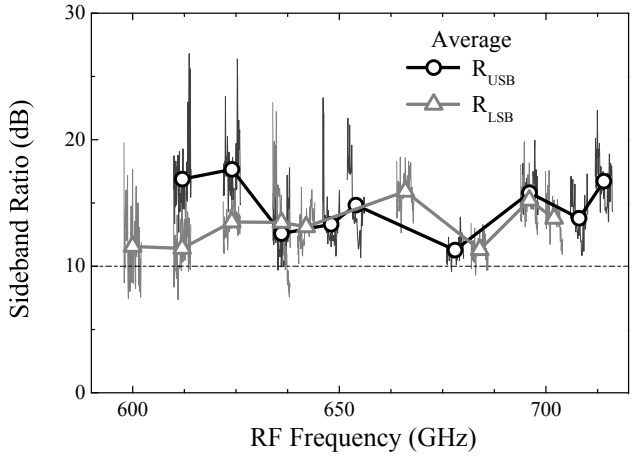

Fig. 12. Sideband ratios of the two IF outputs at different LO frequencies when AlO_x junctions are used. ALMA specification, as described in the text, are summarized by the horizontal dashed line. More than 95 % of the operation points comply with ALMA specification.

exceeds 10 dB. The obtained sideband ratios are in close agreement with the modeling prediction given in the gray line of Fig. 7 if amplitude and phase mismatches of 1.5 dB and 5° in the IF hybrid are considered. This is consistent with the experimental values obtained for the IF hybrid at 77 K, which shows an imbalance in excess of 1 dB and 4° in phase across the $4-8$ GHz band [2]. Note that the commercial hybrid [33] has been optimized for operation at ambient temperature. To investigate the effect of an improved IF hybrid, we have repeated the calculations assuming an imbalance of 0.5 dB and 3°. In that case, an improvement of 3-5 dB is expected (dashed line of Fig. 7) across the whole band. In the event of a perfect IF hybrid the sideband ratio is found to be larger

[2]F. P. Mena and A. Baryshev, Netherlands Institute for Space Research, The Netherlands, unpublished results

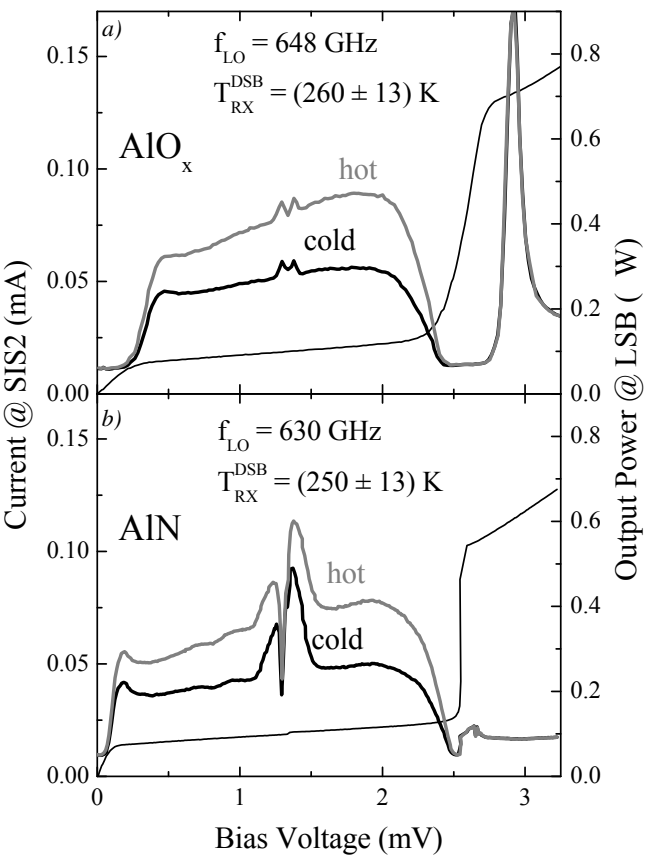

Fig. 13. Measured heterodyne response of the LSB channel of the receiver mounted, *a)*, with AlO_x junctions at an LO frequency of 648 GHz and, *b)*, with AlN junctions at an LO frequency of 630 GHz. The corresponding DSB receiver noise temperature are 260 and 250 K. Notice that for these measurements, both junctions were biased simultaneously at the same voltage. For reference, the associated pumped ($\alpha \approx 0.6$) curves are shown.

than 20 dB. It is expected that such a design may soon be realizable by direct digital processing of the IF.

D. Heterodyne Response

The experimental setup of Fig. 11 can be easily modified to measure the heterodyne response of the system. By removing the beam splitter, *i.e.* the RF insertion, the setup reduces to the conventional variable load method. As an example of these measurements, we show in Fig. 13 the heterodyne response measured at the LSB channel of the receiver when containing AlO_x and AlN junctions. To calculate the noise temperatures we have used the Callen & Welton formulation [34], [35] to determine the temperatures of the noise sources but have not taken into account the finite reflectivity of the absorber (estimated to be less than 1%). However, the induced errors due to this imperfection is only a few degrees which is much smaller than the measurement uncertainty, calculated to be 13 K in the frequency range of interest [36].

We can gain further insight in the behavior of the mixer by studying the LO-pumped I-V curves of Fig. 13. We have done this analysis for AlO_x. From a fit, we calculate the LO pumping parameter α and the RF junction admittance [26]. With this information, and considering the superconducting RF tuning

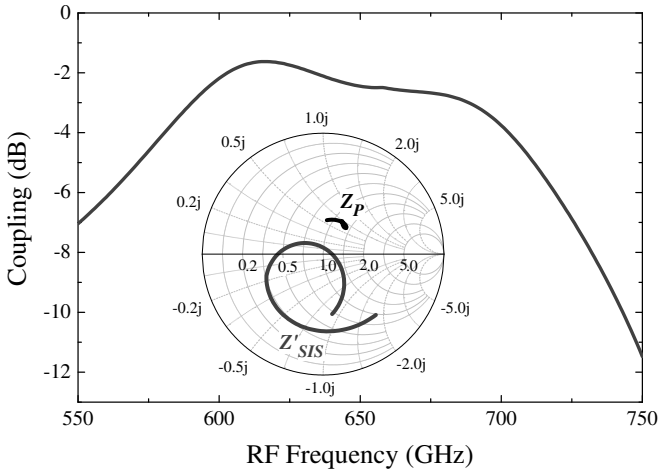

Fig. 14. Calculated coupling between the LO-pumped AlO_xbarrier SIS junction (2.1 mV) and the radial probe waveguide-to-microstrip transition using actual constructed mixer block dimensions. *Inset:* Complex impedance between 600 and 720 GHz of the radial probe ("as measured") and of the LO pumped SIS junction referenced to the throat of the radial probe waveguide transition (Z'_{SIS}) with $\alpha = eV_{LO}/\hbar\omega = 0.6$.

structure shunted by a 80 fF geometric junction capacitance, we are able to de-embed the RF junction impedance to the radial probe waveguide transition reference plane (Z'_{sis}). This impedance is plotted in the inset of Fig. 14 together with the "as built" [7] waveguide-to-microstrip transition impedance Z_p. For optimal coupling $Z'^{*}_{sis} = Z_p$ which, given a locus of 35 + $i17\Omega$, provides a coupling efficiency of 63 % (-2 dB) over the $600-720$ GHz ALMA band 9 frequency band. Please note that the AlO_x barrier SIS design is based on a 40 Ω waveguide transition impedance locus. The RF coupling loss due to the difference between the "theoretical" vs. "actual" probe impedance is $\sim$ 0.75 dB.

E. Noise Temperature

The variable wide-band black-body-radiator load method presented in the previous section allows to determine the noise temperature at the two IF channels, T^{DSB}_{rec}. It has to be noted that the IF power response measured in this way contains contributions from both sidebands and that the resulting noise temperature corresponds to a DSB quantity [31]. The pure single-sideband (SSB) noise temperature is obtained from the DSB quantity via [31]

$$T^{SSB}_{rec} = T^{DSB}_{rec}\left(1 + \frac{1}{R}\right) \ , \qquad (4)$$

where the appropriate sideband ratio R has to be used. Note, however, that with a sideband ratio in excess of 10 dB, this correction amounts to less than 10 %. The uncorrected SSB noise temperatures calculated in such a way for different pumping frequencies are presented in Fig. 15. Regarding this quantity, ALMA specifications for band 9 requires that T_{SSB} must not exceed 335 K over the 80 % range of the nominal bandwidth that has the best performance, whereas 500 K may not be exceeded at any frequency within the nominal bandwidth [8]. The latter specification is presented in the same

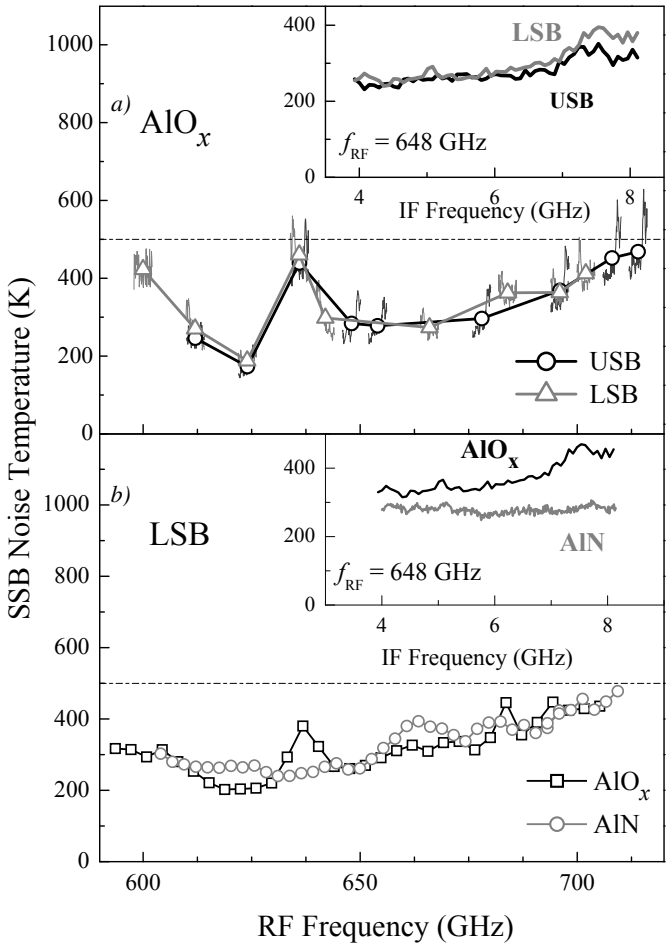

Fig. 15. Uncorrected single-sideband noise temperatures. *a)* Noise temperatures at the two IF outputs with the use of AlO_x junctions. *b)* Comparison of the noise temperatures, at the same IF channel (LSB), for both AlO_x and AlN-barrier junctions. The insets present the data as a function of IF frequency for an RF frequency of 648 GHz (i.e. $f_{LO,USB} = 642$ GHz and $f_{LO,LSB} = 654$ GHz). In this scale, the error bars have the size of the symbols used. As described in the text, both types of junctions were not perfectly matched with the IF circuit and, therefore, the average noise temperatures are similar in both cases. However, the IF response is different as the length of the connecting bond wires was different (0.9 mm for the AlO_x junctions and 0.4 mm for AlN junctions). The bond wires used with the AlN junctions, being shorter, resulted in a flatter behavior of the noise temperature. See also Fig. 8.

Figure as a dashed horizontal line. From our data we see that the performance is excellent, 50 % of the points are below 335 K and 90 % below 500 K. However in an actual ALMA receiver setup the noise temperature may be expected to be reduced by approximately 30 K via the use of a cooled (90 K) multiplier. With such reduction, our sideband-separating mixer would be completely compliant with the ALMA specifications.

Some caution is adviced when comparing the presented SSB results with, for example, the official ALMA Band-9 DBS mixer [37] and HIFI Band-1 and Band-2 mixers [38] on the Herschel Space Observatory [39]. In the case of the ALMA Band-9 DBS mixer, the average measured receiver noise temperature across the band is $\sim$100 K. This is however with a cooled (90 K) last stage multiplier. Comparison to the HIFI mixers is complicated by the use of a cooled LO (80 K),

TABLE VII
MEASURED AND CALCULATED RECEIVER PARAMETERS, WITH ALO_xBARRIER JUNCTIONS, AT $f_{RF} = 648$ GHZ AND $V_{BIAS1} = V_{BIAS2} = 2.1$ MV.

Parameter	USB/LSB
T_{rec}^{SSB} (K)	260 ± 13
T_{opt} (K)	9 ± 3
T_{IF} (K) †	8.5 ± 1
T_{mix} (K)	173 ± 30
G_{mix}^{DSB} (dB) ‡	-9 ± 1
G_{opt} (dB)	-0.25 ± 0.1
$T_{mix}/(G_{opt})$ (K)	184 ± 32
$T_{IF}/(G_{opt}G_{mix}^{DSB})$(K)	67 ± 27
Measured α_{SIS1}	0.60
Measured α_{SIS2}	0.62

† Corrected for IF reflection.
‡ Including Ohmic loss in RF and IF.

lack of IR blocking and vacuum windows (the calibration loads are in a vacuum at 4 K and 90 K), and the fact that ALMA B9 (600-720 GHz) covers the upper part of HIFI mixer Band-1 and the lower part of HIFI mixer Band-2. In the 600-720 GHz frequency range the HIFI in flight DSB sensitivity ranges from 85 K to 140 K.

The insets of Fig. 15 shows a typical dependence of the receiver noise temperature as function of the IF frequency. First, let us concentrate on the inset of Fig. 15*a* where the IF response of both sideband channels, for AlO_x is shown. In this case the noise temperature is rather flat up to a frequency of ~ 7 GHz after which a rise of ~ 120 K is apparent. This behavior can be understood from our simulations presented in Fig. 8. As explained in Section II-E, the original circuit board design was based a 0.3-0.4 mm IF wirebond length. However, it was discovered that a wirebond contact length of ~ 0.9 mm was employed. Unfortunately, the higher than expected wirebond inductance resonates with the parasitic junction capacitance, thin-film RF matching network and RF choke as shown in Fig. 8*b*. Having understood the problem, we have made modifications to the sideband-separating mixer block that allow placing shorter wire bonds. Measurements with high current density AlN-barrier SIS junctions and a 0.4 mm IF contact confirm that the resonance has indeed been pushed out of the IF band as it can be seen in the inset of Fig. 15*b*.

F. Noise Temperature Contributions

The receiver noise temperature, T_{rec}^{DSB}, at an specific output channel, contains contributions from the optics in front of the mixer, loss from the sideband-separating mixer itself, and from the IF chain connected to the mixer. This breakdown is given by

$$T_{rec}^{DSB} = T_{opt} + \frac{T_{mix}^{DSB}}{G_{opt}} + \frac{T_{IF}}{G_{opt}G_{mix}^{DSB}} \ , \qquad (5)$$

where G_{opt} and T_{opt} are the gain and noise temperature of the optics in front of the mixer, G_{mix}^{DSB} and T_{mix}^{DSB} the conversion gain and intrinsic noise temperature of the mixer, and T_{IF} the noise temperature of the IF chain. These quantities were calculated as described below, and are compiled in Table VII.

In front of the mixer's RF port, a window and two heat filters are placed. The window is an antireflection-coated quartz window constructed by QMC [40] following a design that has an optimized transmission to cover the frequency range of band 9 [41]. Moreover, to maximize the hold time of the cryostat, heat filters [42] were placed at the two thermal shields of the cryostat (77 and 4 K, respectively). Provided their respective transmission [40], [43] and physical temperature, the noise temperature of the optical system is calculated to be 9 K.

To determine the contribution from the IF chain we use the characteristics of the AlO_x junctions above the gap voltage as a calibrated shot noise source [44]. An important point to consider is that the power measured in this way contains contributions from both junctions as the signals are mixed in the -3 dB 90° IF hybrid,

$$P_{meas}(V_1, V_2) = \frac{P_{SIS1}(V_1)}{2} + \frac{P_{SIS2}(V_2)}{2} \ . \qquad (6)$$

Given the good reproducibility of our junctions (see Fig. 10), we have assumed that both junctions contribute equal to the total power, except for the noise generated by the extra 1 Ω contact resistance of one of the devices. This extra noise can be estimated by biasing one of the junctions at a particular bias voltage and measuring the generated power as function of the bias voltage of the other junction, then the role of the junctions is interchanged. The difference between them gives the extra noise which is subtracted from the shot noise analysis of the data shown in Fig. 13. The result is an estimated IF noise temperature (corrected for mismatch reflections) of 8 K for both the USB and LSB output ports. The mixer gain and intrinsic noise temperature were also calculated and are presented in Table VII [44], [45].

In future designs it is not unrealistic to expect an improvement in the mixer conversion gain of up to 1.5 dB with a more optimized SIS junction RF coupling design, better matched IF load termination, and on chip integrated IF matching network [29]. In this scenario we estimate an improvement of ~ 34 K in the measured SSB noise temperature of Fig. 15. Ohmic loss in the waveguide structure, estimated from our measurements is in the order of 0.75 to 1.5 dB, and loss in the IF matching network/output-hybrid will remain. Only improved micromaching or electroplating techniques are liable to reduce the front end loss. Loss simulations [15] with perfect waveguide walls and with a conductivity equal to that of gold with a residual-resistivity-ratio of 10 (corresponding to cooling to liquid Helium temperature) indicate a minimum front end loss of 0.37 dB.

V. CONCLUSION

In this article we have presented the design, modeling and construction of a sideband-separating mixer that covers the frequency range of ALMA band 9 ($600 - 720$ GHz). A full test of the mixer and receiver performance has been presented. It was found that the performance is excellent when compared with ALMA specifications. More than 95 % of the operational bandwidth is above the specified sideband ratio (10 dB) and below the specified noise temperature (500 K).

By analyses, the receiver is found to be fully compliant if a cooled (90 K) multiplier could have been used. Moreover it was demonstrated that a better IF match and an improved RF match to the waveguide will make it easier to meet the ALMA specifications.

ACKNOWLEDGMENT

The authors wish to thank B. Jackson and C. Major, SRON, for reading early versions of the manuscript, M. Bekema, SRON, for her diligent help in soldering various components in the mixer and the cryostat, and K. Kaiser, SRON, for his help in machining the cryostat components.

REFERENCES

[1] S. -K. Pan, A. R. Kerr, M. W. Pospiezalski, E. F. Lauria, W. K. Crady, N. Horner, Jr., S. Srikanth, E. Bryerton, K. Saini, S. M. X. Claude, C. C. Chin, P. Dindo, G. Rodrigues, D. Derdall, J. Z. Zhang, and A. W. Lichtenberger, "A Fixed-Tuned SIS Mixer with Ultra-Wide-Band IF and Quantum-Limited Sensitivity for ALMA Band 3 (84-116 GHz) Receivers," in *Proc. 15th Int. Symposium on Space Terahertz Technology,* 2004, pp. 62-69.

[2] A. Navarrini, B. Lazareff, D. Billon-Pierron, and I. Peron, "Design and characterization of 225-370 GHz DSB and 250-360 GHz SSB full height waveguide SIS mixers," in *Proc. 13th Int. Symposium on Space Terahertz Technology,* 2002, pp. 33-40.

[3] D. Maier, S. Devoluy, M. Schicke, and K. F. Schuster "230 GHz SSB SIS Mixer for Band 3 of the new Generation Receivers for the Plateau de Bure Interferometer," in *Proc. 16th Int. Symposium on Space Terahertz Technology,* 2005, S03-02.

[4] D. Maier, A. Barbier, B. Lazareff, and K. F. Schuster, "The Alma Band 7 Mixer," in *Proc. 16th Int. Symposium on Space Terahertz Technology,* 2005, S08-02.

[5] R. Hesper, B. D. Jackson, A. M. Baryshev, J. Adema, K. Wielinga, M. Kroug, T. Zijlstra, G. Gerlofsma, M. Bekema, K. Keizer, H. Schaeffer, J. Barkhof, F. P. Mena, A. Koops, R. Rivas, T. M. Klapwijk, and W. Wild, "Design and development of a 600-720 GHz receiver cartridge for ALMA Band 9," in *Proc. 16th Int. Symposium on Space Terahertz Technology,* 2005, pp.110.

[6] Wenlei Shan, Shengcai Shi, T. Matsunaga, M. Takizawa, A. Endo, T. Noguchi, and Y. Uzawa, "Design and Development of SIS Mixers for ALMA Band 10," *IEEE Transactions on Applied Superconductivity,* vol. 17, pp. 363-366, June 2007.

[7] Radiometer Physics GmbH, Meckenheim, Germany. [Online]. Available: http://www.radiometer-physics.de.

[8] W. Wild and J. Payne (Dec. 2000). ALMA Specification: Specifications for the ALMA Front End Assembly. NRAO, Charlottesville, VA. [Online]. Available: http://www.cv.nrao.edu/∼awootten/mmaimcal/asac/ALMA_rx_specs_V10.pdf.

[9] F. P. Mena and A. Baryshev, "Design and Simulation of a Waveguide Load for ALMA-band 9," NRAO, Charlottesville, VA, ALMA Memo 513, Jan. 2005. [Online]. Available: http://science.nrao.edu/alma/aboutALMA/Technology/ALMA_Memo_Series/main_alma_memo_series.shtml.

[10] F. P. Mena, J. W. Kooi, A. M. Baryshev, C. F. J. Lodewijk, R. Hesper, W. Wild, and T. M. Klapwijk, "An SIS-based sideband-separating heterodyne mixer optimized for the 600 to 720 GHz band," in *8th European Conference on Applied Superconductivity,* Journal of Physics: Conference Series, vol. 97, pp. 012331, 2008.

[11] F. P. Mena, J. W. Kooi, A. M. Baryshev, C. F. J. Lodewijk, R. Hesper, W. Wild, and T. M. Klapwijk, "Construction of a Side-Band-Separating Heterodyne Mixer for Band 9 of ALMA," presented at the *18th Int. Symposium on Space Terahertz Technology,*Pasadena, USA, March 21-23 2007.

[12] F. P. Mena, J. W. Kooi, A. M. Baryshev, C. F. J. Lodewijk, T. M. Klapwijk, W. Wild, V. Desmaris, D. Meledin, A. Pavolotsky, and V. Belitsky, "RF Performance of a 600 − 720 GHz Sideband-Separating Mixer with All-Copper Micromachined Waveguide Mixer Block," presented at the *19th Int. Symposium on Space Terahertz Technology,*Groningen, The Netherlands, Apr. 28-30 2008.

[13] J. W. Kooi, A. Kovács, B. Bumble, G. Chattopadhyay, M. L. Edgar, S. Kaye, R. LeDuc, J. Zmuidzinas, and T.G. Phillips, "Heterodyne Instrumentation Upgrade at the Caltech Submillimeter Observatory," in *Proc. SPIE Conf. Millimeter and submillimeter detectors for Astronomy II,* 2004, vol. 5498, pp. 332-348.

[14] Microwave Office, Applied Wave Research Inc. El Segundo, CA 90245, USA.

[15] Ansoft Corporation, Four Station Square, Suite 200, Pittsburgh, PA 15219-1119, USA.

[16] Microwave Studio, Connecticut, MA, USA (2006). [Online]. Available: http://www.cst.com/.

[17] S. M. X Claude and C. T. Cunningham, "Design of a Sideband-Separating Balanced SIS Mixer Based on Waveguide Hybrids," NRAO, Charlottesville, VA, ALMA Memo 316, Sep. 2000. [Online]. Available: http://science.nrao.edu/alma/aboutALMA/Technology/ALMA_Memo_Series/main_alma_memo_series.shtml.

[18] A. R. Kerr, H. Moseley, E. Wollack, W. Grammer, G. Reiland, R. Henry, and K. P. Stewart,"MF-112 and MF-116: Compact Waveguide Loads and FTS Measurements at Room Temperature and 5 K," NRAO, Charlottesville, VA, ALMA Memo 494, May 2004. [Online]. Available: http://science.nrao.edu/alma/aboutALMA/Technology/ALMA_Memo_Series/main_alma_memo_series.shtml.

[19] G. A. Ediss, A. R. Kerr, H. Moseley, and K. P. Stewart, "FTS Measurements of Eccosorb MF112 at Room Temperature and 5 K from 300 GHz to 2.4 THz," NRAO, Charlottesville, VA, ALMA Memo 273, Sep. 1999. [Online]. Available: http://science.nrao.edu/alma/aboutALMA/Technology/ALMA_Memo_Series/main_alma_memo_series.shtml.

[20] J. W. Kooi, G. Chattopadhyay, S. Withington, F. Rice, J. Zmuidzinas, C. Walker, and G. Yassin, "A Full-Height Waveguide To Thin-Film Microstrip Transition With Exceptional RF Bandwidth And Coupling Efficiency," *Int. J. Ir & Mm Waves,* vol. 24, no. 3, pp. 261-284, Mar. 2003.

[21] C. Risacher, V. Vassilev, A. Pavolotsky, and V. Belitsky, "Waveguide-to-Microstrip Transition with Integrated Bias-T," *IEEE Micro. and Wire. Comp. Lett.,* vol. 13, pp. 262, Jul. 2003.

[22] J. Kawamura, D. Miller, J. Chen, J. Zmuidzinas, B. Bumble, H G. LeDuc, and J. A. Stern, "Very high-current-density Nb/AlN/Nb tunnel junctions for low-noise submillimeter mixers," *Appl. Phys. Lett.,* vol. 76, pp. 2119-2121, Apr. 2000.

[23] T. Zijlstra, C. F. J. Lodewijk, N. Vercruyssen, F. D. Tichelaar, D. N. Loudkov, and T. M. Klapwijk, "Epitaxial aluminum nitride tunnel barriers grown by nitridation with a plasma source," *Appl. Phys. Lett.,* vol. 91, pp. 233102, Dec. 2007.

[24] A. R. Kerr and S.-K. Pan, "Some Recent Developments In The Design Of SIS Mixers," *Int. J. Ir & Mm Waves,* vol. 11, no. 10, pp. 1169-1187, Oct. 1990.

[25] J. W. Kooi, F. Rice, G. Chattopadhyay, S. Sundarum, S. Weinreb and T. G Phillips, "Regarding the IF Output Conductance of SIS Tunnel Junctions and the Integration with Cryogenic InP MMIC Amplifiers," in *Conf. Proc. 10th Int. Symposium on Space Terahertz Technology,* 1999, pp. 100-101.

[26] J. R. Tucker, and M. J. Feldman, "Quantum Detection at Millimeter Wavelengths," in *Rev. Mod. Phys.,* vol. 57, pp. 1055-1113, Oct. 1985.

[27] C. F. J. Lodewijk, M. Kroug, T. M. Klapwijk, F. P. Mena, A. M. Baryshev, and W. Wild, "Improved design for low noise Nb SIS devices for Band 9 of ALMA (600−720 GHz)," in *Conf. Proc. 16th Int. Symposium on Space Terahertz Technology,* 2005 pp. 42-45.

[28] W. Menzel, L. Zhu, K. Wu, F. Bögelsack, "On the design of novel compact broadband planar filters," *IEEE Trans. Microwave Theory Tech.,* vol. 51, no. 2, pp. 364-370, Feb. 2003.

[29] J. W. Kooi, A. Kovács, M. C. Sumner, G. Chattopadhyay, R. Ceria, D. Miller, B. Bumble, H. G. LeDuc, J. A. Stern, and T. G. Phillips, "A 275–425 GHz Tunerless Waveguide Receiver Based on AlN-Barrier SIS Technology," *IEEE Trans. Microw. Theory Tech.,* vol. 55, no. 10, pp. 2086-2096, Oct. 2007.

[30] V. Desmaris, D. Meledin, A. Pavolotsky, R. Monje, and V. Belitsky, "All-metal micromachining for the fabrication of sub-millimetre and THz waveguide components and circuits," *J. Micromech. Microeng.,* Art. ID 095004, vol. 18, 2008.

[31] A. R. Kerr, S.-K. Pan, and J. E. Effland, "Sideband Calibration of Millimeter-Wave Receivers," NRAO, Charlottesville, VA, ALMA Memo 357, Mar. 2001. [Online]. Available: http://science.nrao.edu/alma/aboutALMA/Technology/ALMA_Memo_Series/main_alma_memo_series.shtml.

[32] Eccosorb AN-72, Emmerson&Cumming, Randolph, MA, USA, 2007. [Online]. Available: http://www.eccosorb.com.

[33] ATMh915, ATM Inc., Patchogue, NY, USA, 2007. [Online]. Available: http://www.atmmicrowave.com.

[34] H. B. Callen and T. A. Welton, "Irreversibility and generalized Noise", Phys. Rev., Vol. 83, no. 1, pp. 34-40, Jul., (1951).

[35] A. R. Kerr, "Suggestions for Revised Definitions of Noise Quantities, including Quantum effects", IEEE Trans. Microwave Theory and Techniques, Vol. 47, No. 3, pp. 325-329, Mar., (1999).

[36] "Evaluation of measurement data — Guide to the expression of uncertainty in measurement," Working Group 1 of the Joint Committee for Guides in Metrology, JCGM 100:2008, 2008. [Online]. Available: http://www.bipm.org/utils/common/documents/jcgm/JCGM_100_2008_E.pdf.

[37] A. M. Baryshev, R. Hesper, F. P. Mena, B.D. Jackson, J. Adema, J. Barkhof, W. Wild, M. Candotti, M. Whale, C. Lodewijk, D. Loudkov, T. Zijlstra, T. M. Klapwijk, "Performance of ALMA band 9 receiver series", presented at the *18^{th} Int. Symposium on Space Terahertz Technology,* Pasadena, USA, March 21-23 2007.

[38] Th. de Graauw, F. P. Helmich, T. G. Phillips, J. Stutzki, E. Caux, N. D. Whyborn, P. Dieleman, P. R. Roelfsema, H. Aarts, R. Assendorp, R. Bachiller, W. Baechtold, A. Barcia, D. A. Beintema, V. Belitsky, A. O. Benz, R. Bieber, A. Boogert, C. Borys, B. Bumble, P. Caïs, M. Caris, P. Cerulli-Irelli, G. Chattopadhyay, S. Cherednichenko, M. Ciechanowicz, O. Coeur-Joly, C. Comito, A. Cros, A. de Jonge, G. de Lange, B. Delforges, Y. Delorme, T. den Boggende, J.-M. Desbat, C. Diez-González, A. M. Di Giorgio, L. Dubbeldam, K. Edwards, M. Eggens, N. Erickson, J. Evers, M. Fich, T. Finn, B. Franke, T. Gaier, C. Gal, J. R. Gao, J.-D. Gallego, S. Gauffre, J. J. Gill, S. Glenz, H. Golstein, H. Goulooze, T. Gunsing, R. Güsten, P. Hartogh, W. A. Hatch, R. Higgins, E. C. Honingh, R. Huisman, B. D. Jackson, H. Jacobs, K. Jacobs, C. Jarchow, H. Javadi, W. Jellema, M. Justen, A. Karpov, C. Kasemann, J. Kawamura, G. Keizer, D. Kester, T. M. Klapwijk, Th. Klein, E. Kollberg, J. W. Kooi, P.-P. Kooiman, B. Kopf, M. Krause, J.-M. Krieg, C.Kramer, B. Kruizenga, T. Kuhn, W. Laauwen, R. Lai, B. Larsson, H. G. Leduc, C. Leinz, R. H. Lin, R. Liseau, G. S. Liu, A. Loose, I. Lpez-Fernandez , S. Lord, W. Luinge, A. Marston, J. Martín-Pintado, A. Maestrini, F. W. Maiwald, C. McCoey, I. Mehdi, A. Megej, M. Melchior, L. Meinsma, H. Merkel, M. Michalska, C. Monstein, D. Moratschke, P. Morris, H. Muller, J. A. Murphy, A. Naber, E. Natale, W. Nowosielski, F. Nuzzolo, M. Olberg, M. Olbrich, R. Orfei, P. Orleanski, V. Ossenkopf, T. Peacock, J. C. Pearson, I. Peron, S. Phillip-May, L. Piazzo, P. Planesas, M. Rataj, L. Ravera, C. Risacher, M. Salez, L. A. Samoska, P. Saraceno, R. Schieder, E. Schlecht, F. Schlöder, F. Schmülling, M. Schultz, K. Schuster, O. Siebertz, H. Smit, R. Szczerba, R. Shipman, E. Steinmetz, J. A. Stern, M. Stokroos, R. Teipen, D. Teyssier, T. Tils, N. Trappe, C. van Baaren, B.-J. van Leeuwen, H. van de Stadt, H. Visser, K. J. Wildeman, C. K. Wafelbakker, J. S. Ward, P.Wesselius, W. Wild, S. Wulff, H.-J.Wunsch, X. Tielens, P. Zaal, H. Zirath, J. Zmuidzinas, and F. Zwart, "The Herschel-Heterodyne Instrument for the Far-Infrared (HIFI)", Astronomy & Astrophysics 518, L6, 2010.

[39] G. L. Pilbratt, J. R. Riedinger, T. Passvogel, G. Crone, D. Doyle, U. Gageur, A. M. Heras, C. Jewell, L. Metcalfe, S. Ott, and M. Schmidt, "Herschel Space Observatory. An ESA facility for far-infrared and submillimetre astronomy", Astronomy & Astrophysics 518, L1, 2010.

[40] QMC Instruments Ltd., Cardiff, UK, 2007. [Online]. Available: http://www.terahertz.co.uk.

[41] D. Koller, A. R. Kerr, G. A. Ediss, "Proposed Quartz Vacuum Window Designs for ALMA Bands 3–10," NRAO, Charlottesville, VA, ALMA Memo 397, Jun. 2003. [Online]. Available: http://science.nrao.edu/alma/aboutALMA/Technology/ALMA_Memo_Series/main_alma_memo_series.shtml.

[42] GORE-TEX GR sheet gasketing, according DIN 28091, TF-0-0. [Online]. Available: http://www.gore.com.

[43] A. M. Baryshev, M. Candotti, and N. A. Trappe, "Cross-polarization characterization of GORE-TEX slabs at band 9 frequencies," NRAO, Charlottesville, VA, ALMA Memo 551, Jun. 2006. [Online]. Available: http://science.nrao.edu/alma/aboutALMA/Technology/ALMA_Memo_Series/main_alma_memo_series.shtml.

[44] D. P. Woody, R. E. Miller, and M. J. Wengler, "$85-115$-GHz receivers for radio astronomy," *IEEE Trans. Microwave Theory Tech.,* vol.33, no. 2, pp. 90–95, Feb. 1985.

[45] M. J. Wengler, and D. P. Woody, "Quantum Noise in Heterodyne Detection," *IEEE J. Quantum Electronics,* vol. QE-23, no.5, pp. 613-622, May 1987.

F. P. Mena Received his B.S. degree in Physics from Escuela Politécnica Nacional, Quito-Ecuador, in 1994, the M.S. and Ph.D. degrees in Physics from University of Groningen, The Netherlands, in 2000 and 2004, respectively.

In 2004 he joined the Netherlands Institute for Space Research (SRON) as Instrument Scientist at the Low Energy Division. Since 2008, he is Assitant Professor at the Electrical Engineering Department of Universidad de Chile.

J. W. Kooi Biography not available at the moment.

A. M. Baryshev Biography not available at the moment.

C. F. J. Lodewijk Biography not available at the moment.

T. Zijlstra Biography not available at the moment.

R. Hesper Biography not available at the moment.

G. Gerlofsma Biography not available at the moment.

T. M. Klapwijk Biography not available at the moment.

W. Wild Biography not available at the moment.